Available online at www.sciencedirect.com

ScienceDirect

Energy Procedia 126 (201709) 26–33

Energy Procedia

www.elsevier.com/locate/procedia

72nd Conference of the Italian Thermal Machines Engineering Association, ATI2017, 6-8 September 2017, Lecce, Italy

Natural convection from a pair of differentially-heated horizontal cylinders aligned side by side in a nanofluid-filled square enclosure

Alessandro Quintino, Elisa Ricci, Emanuele Habib, Massimo Corcione*

DIAEE Sezione Fisica Tecnica - Sapienza Università di Roma, via Eudossiana 18, 00184 Rome, Italy

Abstract

A two-phase model based on the double-diffusive approach is used to perform a numerical study on natural convection from a pair of differentially-heated horizontal cylinders set side by side in a nanofluid-filled adiabatic square enclosure. The study is conducted under the assumption that Brownian diffusion and thermophoresis are the only slip mechanisms by which the solid phase can develop a significant relative velocity with respect to the liquid phase. The system of the governing equations of continuity, momentum and energy for the nanofluid, and continuity for the nanoparticles, is solved by the way of a computational code which incorporates three empirical correlations for the evaluation of the effective thermal conductivity, the effective dynamic viscosity, and the thermophoretic diffusion coefficient, all based on a wide number of literature experimental data. The pressure-velocity coupling is handled through the SIMPLE-C algorithm. Simulations are executed for three different nanofluids, using the diameter and the average volume fraction of the suspended nanoparticles, as well as the cavity width, the inter-cylinder spacing, the average temperature of the nanofluid, and the temperature difference imposed between the cylinders, as controlling parameters, whose effects are thoroughly analyzed and discussed. It is found that the impact of the nanoparticle dispersion into the base liquid increases remarkably with increasing the average temperature, whereas it increases just moderately as the nanoparticle size decreases, as well as the imposed temperature difference and the cavity width increase. Conversely, the distance between the cylinders seems to have marginal effects. Moreover, an optimal particle loading for maximum heat transfer is detected for most configurations investigated.

Peer-review under responsibility of the scientific committee of the 72nd Conference of the Italian Thermal Machines Engineering Association

*Keywords:*Nanofluid; Natural convection; Differentially-heated horizontal cylinders; Two-phase modeling; Enhanced heat transfer; Optimal particle loading.

* Corresponding author. Tel.: +39 0644585443
E-mail address: massimo.corcione@uniroma1.it

1876-6102
Peer-review under responsibility of the scientific committee of the 72nd Conference of the Italian Thermal Machines Engineering Association
10.1016/j.egypro.2017.08.050

Nomenclature

c	specific heat at constant pressure, J/(kgK)
D	diameter of the cylinders (m)
D_B	Brownian diffusion coefficient, m^2/s
D_T	thermophoretic diffusion coefficient, m^2/s
d_p	nanoparticle diameter, m
$\vec{g}$	gravity vector, m/s^2
$\boldsymbol{I}$	unit tensor
L	inter-cylinder spacing (m)
$\vec{J}_p$	nanoparticle diffusion mass flux, $kg/(m^2s)$
k	thermal conductivity, W/(mK)
k_B	Boltzmann constant = $1.38066 \cdot 10^{-23}$ JK^{-1}
m	nanoparticle mass fraction
Nu	Nusselt number
p	pressure, Pa
Pr	Prandtl number
Q	heat transfer rate, W
q	heat flux, W/m^2
Ra	Rayleigh number
S_T	thermophoresis parameter
T	temperature, K
t	time, s
U	x-wise velocity component, m/s
$\vec{V}$	velocity vector, m/s
V	y-wise velocity component, m/s
$\vec{V}_T$	thermophoretic velocity vector, m/s
W	width of the enclosure, m
x,y	Cartesian coordinates, m

Greek symbols

δ	dimensionless inter-cylinder spacing
θ	angular coordinate, deg
φ	nanoparticle volume fraction
μ	dynamic viscosity, kg/(ms)
ρ	mass density, kg/m^3
$\boldsymbol{\tau}$	stress tensor, $kg/(ms^2)$
λ	dimensionless inter-cylinder spacing

Subscripts

av	average
c	cooled wall, at the temperature of the cooled wall

1. Introduction

Buoyancy-induced convection of nanofluids inside adiabatic enclosures containing heated and cooled cylinders has recently gained a lot of interest, due to its relevance to many potential engineering and science applications, such as solar collectors and heat exchangers, just to name a few.

The studies available in the literature on this topic were carried out numerically by Garoosi and colleagues [1,2], and Khalili et al. [3]. However, both studies executed by Garoosi and colleagues [1,2] are based on the single-phase approach, in which nanofluids are treated as pure fluids, assuming that the solid and liquid phases are in local thermal and hydrodynamic equilibrium, thus neglecting the effects of the slip motion that actually occurs between the suspended nanoparticles and the base liquid. Notice that, as thoroughly discussed in a study recently conducted by Corcione et al. [4], these slip effects can be regarded as responsible for the heat transfer degradation detected experimentally in cavities differentially heated at sides. On the other hand, in the two-phase investigation performed by Khalili et al. [3], the thermophoretic velocity of the suspended nanoparticles is calculated by the way of the McNab-Meisen empirical relation [5], whose applicability to water-based nanofluids with suspended metal oxide nanoparticles has never been demonstrated.

Framed in this background, a comprehensive numerical study on natural convection from a pair of differentially-heated horizontal cylinders set side by side in a nanofluid-filled adiabatic square enclosure is performed using a two-phase model based on the double-diffusive approach. It is assumed that Brownian diffusion and thermophoresis are the only slip mechanisms by which the solid phase can develop a significant relative velocity with respect to the liquid phase. The model developed incorporates three empirical correlations for the calculation of the effective thermal conductivity, the effective dynamic viscosity, and the thermophoretic diffusion coefficient, all based on a high number of experimental data available in the literature from diverse sources, and validated using relations from other authors and experimental data different from those employed in generating them. Scope of the present paper is to evaluate the effects of the nature, size and average volume fraction of the suspended nanoparticles, as well as those of the cavity width, the inter-cylinder spacing, the average temperature of the nanofluid, and the temperature difference imposed between the cylinders, on the nanofluid heat transfer performance.

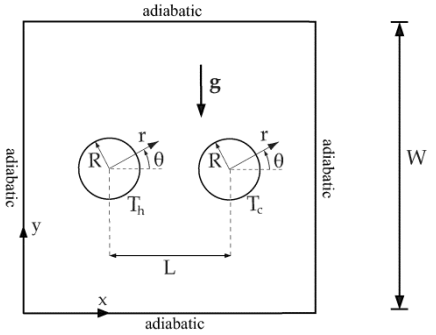

Fig. 1. Sketch of the geometry and coordinate systems.

2. Mathematical formulation

A square enclosure of width W, containing a pair of differentially-heated horizontal cylinders of diameter $D=2R$, is filled with a water-based nanofluid. The cylinders, set side by side at a center-to-center distance L, are kept at two different uniform temperatures T_c and T_h, while the four walls of the cavity are assumed to be perfectly insulated. A sketch of the enclosure is depicted in Fig. 1, wherein the reference polar and Cartesian coordinate systems, for the cylinders and the cavity, respectively, are also represented. The resulting buoyancy-induced flow is considered to be two-dimensional and laminar, with negligible viscous dissipation and pressure work. It is assumed that the suspended nanoparticles and the base liquid are in local thermal equilibrium, and that Brownian diffusion and thermophoresis are the only slip mechanisms by which the nanoparticles can develop a significant relative velocity with respect to the base liquid, as discussed by Buongiorno [6] – Brownian motion takes place from high to low nanoparticle concentrations, whereas thermophoresis occurs in the direction from hot to cold. Another assumption made in the derivation of the model is that the effective physical properties of the nanofluid vary with temperature, other than being locally dependent on the nanoparticle concentration. Finally, the heat transfer associated with the nanoparticle motion relative to the base fluid, as well as radiative heat transfer, are neglected.

In these hypotheses, the governing equations of continuity, momentum and energy for the nanofluid, and the equation of continuity for the nanoparticles, reduce to:

$$\frac{\partial \rho_n}{\partial t} + \nabla \cdot \left(\rho_n \vec{V} \right) = 0 \tag{1}$$

$$\frac{\partial \left(\rho_n \vec{V} \right)}{\partial t} + \nabla \cdot \left(\rho_n \vec{V} \vec{V} \right) = \nabla \cdot \tau + \rho_n \vec{g} \tag{2}$$

$$\frac{\partial \left(\rho_n c_n T \right)}{\partial t} + \nabla \cdot \left(\rho_n \vec{V} c_n T \right) = \nabla \cdot \left(k_n \nabla T \right) \tag{3}$$

$$\frac{\partial \left(\rho_n m \right)}{\partial t} + \nabla \cdot \left(\rho_n \vec{V} m \right) = -\nabla \cdot \vec{J}_p \tag{4}$$

where t is the time, $\vec{V}$ is the velocity vector having radial and tangential components U and V in the polar system and x-wise and y-wise components U and V in the Cartesian system, τ is the stress tensor, $\vec{g}$ is the gravity vector, $\vec{J}_p$ is the nanoparticle diffusion mass flux, T is the temperature, m is the mass fraction (also called concentration) of the suspended nanoparticles, ρ_n is the effective mass density, c_n is the effective specific heat at constant pressure, and k_n is the effective thermal conductivity. The nanoparticle diffusion mass flux is calculated as the sum of the Brownian and thermophoretic diffusion terms in the hypothesis of dilute mixture (i.e., low mass fraction), thus obtaining:

$$\vec{J}_p = -\rho_n \cdot \left(D_B \nabla m + D_T \frac{\nabla T}{T} \right), \tag{5}$$

where D_B and D_T are the Brownian and thermophoretic diffusion coefficients, respectively.

The Brownian diffusion coefficient, D_B, is given by the Stokes–Einstein equation [7]:

$$D_B = \frac{k_B T}{3\pi\pi_f d_p}, \tag{6}$$

in which k_B= 1.38066 × 10^{-23} J/K is the Boltzmann constant, μ_f is the dynamic viscosity of the base fluid, and d_p is the diameter of the suspended nanoparticles.

The thermophoretic diffusion coefficient, D_T, is expressed as

$$D_T = S_T \frac{\mu_f}{\rho_f} m, \tag{7}$$

where ρ_f is the mass density of the base liquid, and S_T is the so-called thermophoresis parameter, that, for water-based nanofluids containing metal oxide nanoparticles, can be evaluated by the following correlation recently developed by Corcione et al. [8] based on experimental data-sets reported in the literature by different research teams:

$$\mathrm{S}_T = \left[\left(1.5 \times 10^4\right) \cdot \left(\frac{k_s}{k_f} \right)^{-3} + 0.9 \right] \cdot \left[-16 \cdot \left(\varphi_{av}\right)^{2.35} + 0.0195 \right], \tag{8}$$

in which k_s and k_f are the thermal conductivities of the solid nanoparticles and the base fluid, respectively, and φ_{av} is the average volume fraction of the suspended nanoparticles.

The effective thermal conductivity, k_n, and the effective dynamic viscosity, μ_n, can be predicted using the correlations reported in [8], while the effective mass density, ρ_n, and the effective specific heat at constant pressure, c_n, are calculated by the customary mixing theory.

The assigned boundary conditions are: (a) $T = T_h$, $\vec{V} = 0$ and $\vec{J}_p = 0$ at the surface of the heated cylinder; (b) $T = T_c$, $\vec{V} = 0$ and $\vec{J}_p = 0$ at the surface of the cooled cylinder; and (c) $\partial T/\partial n = 0$, $\vec{V} = 0$ and $\vec{J}_p = 0$ at the four cavity walls, where n denotes the normal to the wall. The initial conditions assumed throughout the whole enclosure are: (a) nanofluid at rest, i.e., $\vec{V} = 0$; (b) uniform average temperature of the nanofluid, $T_{av} = (T_h + T_c)/2$; and (c) assigned uniform average mass fraction of the suspended nanoparticles, m_{av}.

3. Computational procedure

The system of the governing equations defined by Eqs. (1)–(4), in conjunction with the boundary and initial conditions stated earlier, is solved through a control-volume formulation of the finite-difference method. The pressure-velocity coupling is handled using the SIMPLE-C algorithm, the convective terms are approximated by the QUICK discretization scheme, whereas a second-order backward scheme is applied for time integration. A standard under-relaxation technique is enforced in all steps of the computational procedure to ensure adequate convergence. Within each time-step, the spatial numerical solution of temperature, velocity and concentration fields is considered to be converged when the maximum absolute value of the mass source, as well as the relative changes of the dependent variables at any grid-node between two consecutive iterations, are smaller than the pre-specified values of 10^{-6} and 10^{-7}, respectively. In addition, the condition that the relative difference between the incoming and outgoing heat transfer rates at the heated and cooled walls must be smaller than a pre-assigned value of 10^{-2}, is also applied.

Time-integration is stopped upon reaching steady-state, at which the heat transfer rates at the heated and cooled cylinder surfaces, Q_h and Q_c, can be assumed to be the same, thus meaning

$$Q_h = -Q_c = Q\,, \tag{9}$$

where Q is the rate of heat transferred between the cylinders.

Numerical tests related to the dependence of the results on the mesh spacing and time stepping have been performed for several combinations of the seven controlling parameters, namely m_{av}, d_p, T_c, T_h, D, L, and W. The typical number of nodal points of the polar and Cartesian discretization grids used for simulations lie in the ranges between 100 × 100 and 120 × 120, and between 120 × 120 and 140 × 140, respectively. Moreover, typical time-steps used for simulations lie in the range between 5×10^{-4} s and 10^{-2} s. Finally, full details on the validation of the numerical code used for the present study are available in a recent study performed by Quintino et al. [9].

4. Results and discussion

Numerical simulations are performed using water-based nanofluids with suspended metal oxide nanoparticles, for different values of (a) the average volume fraction of the solid phase, φ_{av}, in the range between 0 and 0.04, (b) the average diameter of the nanoparticles, d_p, in the range between 25 nm and 100 nm, (c) the average temperature of the nanofluid, T_{av}, in the range between 300 K and 330 K, (d) the temperature difference imposed between the cylinders, ΔT, in the range between 5 K and 20 K, (e) the dimensionless cylinder diameter, δ, in the range between 0.1 and 0.3, (f) the dimensionless inter-cylinder spacing, λ, in the range between 0.3 and 0.6, and (g) the width of the enclosure, W, in the range between 0.02 m and 0.06 m.

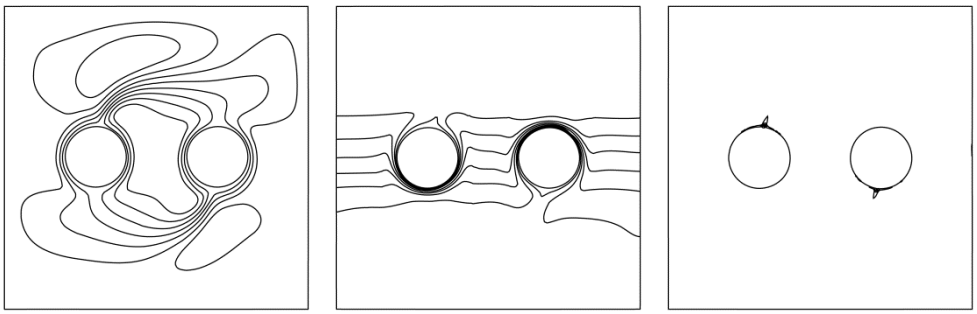

Fig 2. Streamline, isotherm and isoconcentration contours for $Al_2O_3 + H_2O$, $W = 40$ mm, $d_p = 25$ nm, $\varphi_{av} = 0.02$, $\lambda = 0.4$, $\delta = 0.2$, $T_{av} = 315$ K, and $\Delta T = 10$ K.

Typical local results are reported in Fig. 2, in which streamline, isotherm and isoconcentration contours relative to a cavity filled with Al_2O_3+H_2O are plotted for $W = 40$ mm, $d_p = 25$ nm, $\varphi_{av} = 0.02$, $\delta = 0.2$, $\lambda = 0.4$, $T_{av} = 315$ K, and $\Delta T = 10$ K. It is apparent that the flow field consists of a primary circulation occurring between the cylinders, due to the rise of the hot nanofluid adjacent to the heated cylinder and its descent past the opposite cooled cylinder, and of a secondary cell, driven by the same imposed temperature difference, that embraces both cylinders. Moreover, the combined effects of the nanofluid circulation due to the imposed differential heating, and the diffusion of the suspended nanoparticles in the direction from hot to cold, give rise to the formation of a low-concentration boundary layer adjacent to the heated cylinder surface, and a high-concentration boundary layer adjacent to the cooled cylinder surface, which means the establishment of a concentration gradient across the enclosure, whose role in determining the heat transfer performance of the nanofluid needs being discussed. In fact, the nanofluid behavior is primarily affected by the two opposite effects arising from the increase of both the thermal conductivity and the dynamic viscosity produced by the dispersion of the nanoparticles into the base liquid: the first effect, which tends to enhance the nanofluid heat transfer performance, prevails at small volume fractions of the suspended solid phase, whereas the

second effect, which tends to degrade the nanofluid heat transfer performance, prevails at higher volume fractions. On the other hand, due to the mentioned concentration gradient, a cooperating solutal driving force arises. The situation is such that, as a rule, this extra-buoyancy tends to compensate the increased friction consequent to the viscosity growth, thus implying that the beneficial effect of the increased thermal conductivity plays the major role in determining the heat transfer performance of the nanofluid. Hence, on account of Eq. (11), a pronounced heat transfer enhancement has to be expected at high average temperatures, as shown in Fig. 3(a), where a number of distributions of the ratio between the heat transfer rates across the nanofluid and the pure base fluid, Q_n / Q_f, are plotted versus φ_{av} using T_{av} as a parameter. In the same figure, the distribution of Q_n / Q_f versus φ_{av} at T_{av} = 330 K obtained using the single-phase approach, i.e., by simply imposing $D_T = 0$, is also reported for comparison purposes. It can be noticed that the amount of heat exchanged by the nanofluid may be significantly higher than that exchanged by the pure base liquid, which is what happens at T_{av} = 330 K and φ_{av} = 0.04, that, for the examined configuration, corresponds to a 18% enhancement. Conversely, at lower temperatures, e.g. T_{av} = 300 K, the limited increase of the thermal conductivity gives rise to a different situation. In fact, the dispersion of a progressively larger amount of nanoparticles into the base liquid results in a mild increase of the ratio Q_n / Q_f up to a point, which is due to the prevailing effect of the increased thermal conductivity. The value of φ_{av} corresponding to the peak of Q_n / Q_f can be identified as the optimal particle loading for maximum heat transfer, φ_{opt}. As φ_{av} is further increased above φ_{opt}, the ratio Q_n / Q_f decreases, which is a direct consequence of the prevailing effect of the growth of the dynamic viscosity. Moreover, it can be seen that the adoption of the single-phase approach results in a non-negligible underestimation of the heat transfer enhancement.

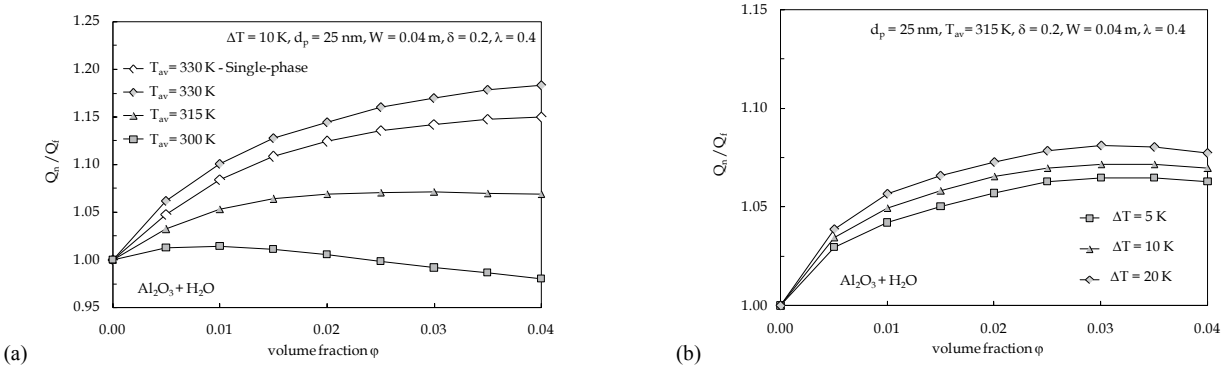

Fig. 3. (a) Distributions of Q_n / Q_f vs. φ_{av} for $Al_2O_3 + H_2O$, W = 40 mm, d_p= 25 nm, λ = 0.4, δ = 0.2, and ΔT = 10 K, using T_{av} as a parameter; and (b) Distributions of Q_n / Q_f vs. φ_{av} for $Al_2O_3 + H_2O$, W = 40 mm, d_p= 25 nm, λ = 0.4, δ = 0.2, and T_{av}= 315 K, using ΔT as a parameter.

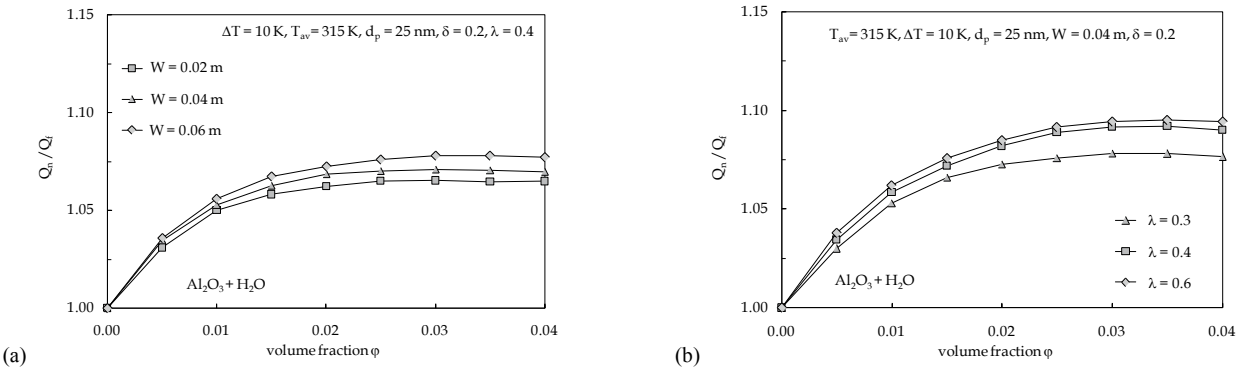

Fig. 4. (a) Distributions of Q_n / Q_f vs. φ_{av} for $Al_2O_3 + H_2O$, d_p = 25 nm, λ = 0.4, δ = 0.2, T_{av}= 315 K, and ΔT = 10 K, using W as a parameter; and (b) Distributions of Q_n / Q_f vs. φ_{av} for $Al_2O_3 + H_2O$, W = 40 mm, d_p= 25 nm, δ = 0.2, T_{av}= 315 K, and ΔT = 10 K, using λ as a parameter.

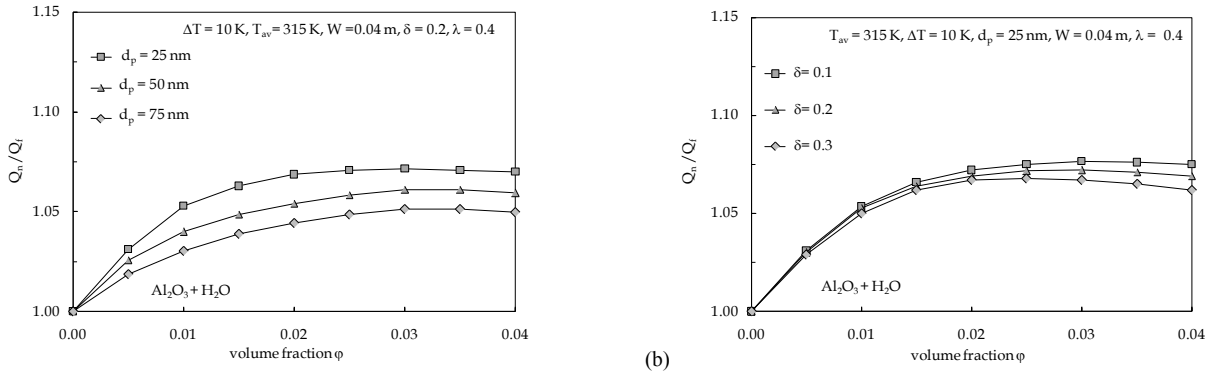

Fig. 5. (a) Distributions of Q_n / Q_f vs. φ_{av} for $Al_2O_3 + H_2O$, $W = 40$ mm, $\lambda = 0.4$, $\delta = 0.2$, $T_{av} = 315$ K, and $\Delta T = 10$ K, using d_p as a parameter; and (b) Distributions of Q_n / Q_f vs. φ_{av} for $W = 40$ mm, $d_p = 25$ nm, $\lambda = 0.4$, $T_{av} = 315$ K, and $\Delta T = 10$ K, using δ as a parameter.

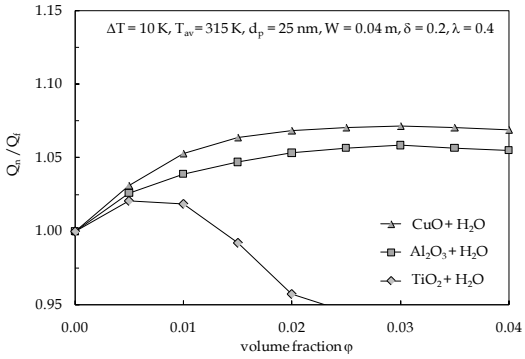

Fig. 6. Distributions of Q_n / Q_f vs. φ_{av} for $W = 40$ mm, $d_p = 25$ nm, $\lambda = 0.4$, $\delta = 0.2$, $T_{av} = 315$ K, and $\Delta T = 10$ K, using the solid phase material as a parameter.

The additional effects on the heat transfer performance of the imposed temperature difference, the cavity width, the cylinder diameter, the inter-cylinder spacing, and the nanoparticle diameter, are pointed out in Figs. 3(b), 4(a), 4(b), 5(a) and 5(b), in which, for any independent variable, a number of distributions of Q_n / Q_f are plotted versus φ_{av} using the variable itself as a parameter. Besides the fact that all these controlling variables have moderate effects, it is apparent that Q_n / Q_f increases as ΔT, W and λ are increased, whereas it decreases with increasing both d_p and δ. Indeed, the strong dependence of Q_n / Q_f on T_{av} underlines that the average temperature is the key parameter that basically determines the enhancement or deterioration of the heat transfer performance of the nanofluid compared with that of the pure base liquid.

Finally, the effects of the nanoparticle material are emphasized in Fig. 6, in which, fixed $d_p = 25$ nm, $W = 40$ mm, $\delta = 0.2$, $\lambda = 0.4$, $T_{av} = 315$ K, and $\Delta T = 10$K, the distributions of Q_n / Q_f plotted versus φ_{av} are depicted for $Al_2O_3 + H_2O$, $CuO + H_2O$ and $TiO_2 + H_2O$, showing that $TiO_2 + H_2O$ exhibits a relative heat transfer performance much lower than $CuO + H_2O$ and $Al_2O_3 + H_2O$, which is ascribable to the lower effective thermal conductivity and the higher thermophoretic diffusion coefficient.

5. Conclusions

Laminar natural convection of nanofluids from a pair of differentially-heated horizontal cylinders set side by side in a nanofluid-filled adiabatic square cavity has been studied numerically by means of a two-phase model based on the double-diffusive approach, in the hypothesis that the slip motion occurring between the solid and liquid phases is due to Brownian diffusion and thermophoresis.

The main results obtained may be summarized as follows:

(a) the dispersion of the solid nanoparticles into the base liquid has its maximum effect on the nanofluid heat transfer performance at an optimal particle loading;

(b) the impact of the nanoparticle dispersion into the base liquid increases remarkably with increasing the average temperature, whereas it increases just moderately as the imposed temperature difference, the cavity width and the inter-cylinder spacing increase, and the nanoparticle size and the cylinder diameter decrease;

(c) at temperatures of the order of the room temperature or just higher, the nanofluid heat transfer performance of $CuO + H_2O$ and of $Al_2O_3 + H_2O$, is much higher than that of $TiO_2 + H_2O$.

References

[1] Garoosi F, Hoseininejad F, Rashidi M M, Numerical study of natural convection heat transfer in a heat exchanger filled with nanofluids, Energy 109 (2016) 664-678.

[2] Garoosi F, Hoseininejad F, Numerical study of natural and mixed convection heat transfer between differentially heated cylinders in an adiabatic enclosure filled with nanofluid, J. Molecular Liquids 215 (2016) 1-17.

[3] Khalili E, Saboonchi A, Saghafian M, Natural convection of Al_2O_3 nanofluid between two horizontal cylinders inside a circular enclosure, Heat Transfer Eng. 38 (2017) 177-189.

[4] Corcione M, Cianfrini M, Quintino A, Temperature effects on the enhanced or deteriorated buoyancy-driven heat transfer in differentially heated enclosures filled with nanofluids, Num. Heat Transfer, Part A 70 (2016) 223-241.

[5] McNab G S, Meisen A, Thermophoresis in liquids, J. Colloid Interface Science 44 (1973) 339–346.

[6] Buongiorno J, Convective transport in nanofluids, J. Heat Transfer– Trans. ASME 128 (2006) 240-250.

[7] Einstein A, Über die von der molekularkinetischen Theorie der Wärme geforderte Bewegung von in ruhenden Flüssigkeiten suspendierten Teilchen (in German), Ann. Phys.17 (1905) 549-560.

[8] Corcione M, Cianfrini M, Quintino A, Enhanced natural convection heat transfer of nanofluids in enclosures with two adjacent walls heated and the two opposite walls cooled, Int. J. Heat Mass Transfer 88 (2015) 902-913.

[9] Quintino A, Ricci E, Corcione M, Thermophoresis-induced oscillatory natural convection flows of water-based nanofluids in tilted cavities, Num. Heat Transfer, Part A 71 (2017) 270-289.